Advanced Composite Materials

ISSN: 0924-3046 (Print) 1568-5519 (Online) Journal homepage: http://www.tandfonline.com/loi/tacm20

Damage growth behavior and interlaminar fracture resistance of CFRP laminates under shear fracture mode

Hiroshi Suemasu & Yusuke Tanikado

To cite this article: Hiroshi Suemasu & Yusuke Tanikado (2015) Damage growth behavior and interlaminar fracture resistance of CFRP laminates under shear fracture mode, Advanced Composite Materials, 24:5, 451-466, DOI: 10.1080/09243046.2014.914998

To link to this article: http://dx.doi.org/10.1080/09243046.2014.914998

Advanced Composite Materials, 2015
Vol. 24, No. 5, 451–466, http://dx.doi.org/10.1080/09243046.2014.914998

Damage growth behavior and interlaminar fracture resistance of CFRP laminates under shear fracture mode

Hiroshi Suemasu[a]* and Yusuke Tanikado[b]

[a]*Faculty of Science and Engineering, Sophia University, Tokyo, Japan;* [b]*Toray Corporation, Otsu, Shiga, Japan*

(*Received 30 September 2013; accepted 10 April 2014*)

Interfacial failure problem of composite laminates was experimentally studied to know the dependence of interlaminar fracture resistance on various conditions as well as conditions of migration of the delamination into lamina to understand three-dimensional complex damage growths. A test method was proposed to realize a stable damage growth without influence of free edge under varying shear fracture mode in laminated composites. We could numerically evaluate critical energy release rate (ERR) for the delamination growth using a finite element method based on the measured shapes of the delamination and the applied load. Not only total ERR but also the ERR components in two directions parallel and normal to the fiber were calculated. The two components of the energy release were more appropriate to discuss the damage growth problem than the mode II and III components. When the normal component to the fiber was relatively small, the total ERR controlled the instability of the delamination. The delamination migrated into the lamina (that is, jumped to the other interface) where the ERR components normal to the fiber reached some level. The migration caused an anchoring effect on the delamination growth.

Keywords: interlaminar fracture resistance; mixed-mode shear; fiber orientation; delamination; crack migration

1. Introduction

Laminated composites are used particularly for aerospace structures due to their high specific strength and stiffness. However, owing to its insufficient interlaminar toughness the laminated composite structures are vulnerable to interlaminar damage under various load conditions such as static, impact, and/or cyclic loads. The damage may cause significant reduction of load-carrying capability even when no fiber damage occurs. So, the interlaminar fracture toughness is regarded as an important measure of the failure tolerance of the laminates. Considering that not only interlaminar normal (mode I) stress fields but also in-plane shear (mode II) and out-of-plane shear (mode III) stress fields cause delamination growth, values of all three individual and/or mixed interlaminar fracture toughnesses or fracture resistances must be evaluated to characterize the interlaminar fracture property of the composite laminates with using appropriate test methods. Migration behavior of delamination into the lamina and/or the deflection of matrix crack to delamination make the interface failure of composite laminates more complex and difficult to be predicted.

*Corresponding author. Email: suemasu@sophia.ac.jp

There are numerous studies concerning the interlaminar toughness as well as test methods to measure it. The mode I fracture toughness of the laminated composites is well measured by DCB (Double Cantilever Beam) test method.[1–3] The mode II fracture toughness of the laminated composite is also obtained through comparatively simple ENF (End Notched Flexure) test method.[4–6] Mixed normal and in-plane shear (mode I and II) fracture test can be also conducted through MMB (Mixed Mode Bending) and CLS (Cracked Lap Shear) test methods.[7,8] There are experimental techniques for measuring mode III proposed by several workers [9–13] such as rail shear test and ECT (Edge Cracked Torsion) test method, which are not so handy as those proposed for measuring mode I and II fracture toughnesses. Szekrényes [14] and de Morais et al. [15] have proposed elaborate test methods to measure mixed mode II and III fracture toughness, respectively. Suemasu et al. [16] has proposed a modified SCB (Split Cantilever Beam) test method easy to conduct and possible to evaluate wide range of mixed mode II and III fracture toughnesses by a single test using finite element method. It enables to measure interlaminar resistance under stable crack growth. The test revealed that the interlaminar fracture behavior under shear mode was extremely complex in the real laminated plate. The damage grew three dimensionally and free edge made the evaluation of the three-dimensional growth condition difficult. It is worth to carry out tests of the interlaminar fracture resistance possible to consider the various effects on interfacial failure behavior such as mixed mode ratio, delamination propagation orientation, coupling with the other damages, migration behavior into the lamina, and its large statistical variation.[17–21]

The authors propose an indentation test method to evaluate interlaminar fracture resistance under the shear-mode fracture conditions without free-edge effect. Since the present test method realizes varying fracture conditions along the crack front under stable delamination propagation condition, the various effects on the interfacial fracture are evaluated and the interface problem under shear fracture condition is discussed through the experimental results.

2. Experiment

The material system tested was CFRP cross-ply laminates ($[90°/0]_{4s}$) (T700/2592SC, Toray), which had moderate interlaminar toughness. The thickness of the laminates was about 4.0 mm. The material properties measured are listed in Table 1. The laminates were cured according to the instruction of the suppliers. G_{Ic} was obtained by DCB test and the two G_{IIc} values were obtained by ENF tests. The fracture resistance of 0/0 interface was measured as usually done using specimens ($[90°/0]_{4s}$) with initial embedded delamination. The fracture resistance of 0/90° interface was measured by setting the specimen ($[0/90°]_8$) so that the 0 and 90° layers were above and below the delaminating interface, respectively. Owing to the present setting, we could make the delamination propagate along the 0/90° interface. The fracture resistance of 0/90° interface was slightly higher than that of

Table 1. Material properties of the unidirectional CFRP.

							G_{IIc} (kJ/m^2)	
E_L (GPa)	E_T (GPa)	G_{LT} (GPa)	G_{TT} (GPa)	v_{LT}	v_{TT}	G_{Ic} (kJ/m^2)	0/0	0/90°
136.0	10.0	5.96	2.7	0.376	0.49	0.34 kJ/m^2	1.0 ± 0.4	1.2 ± 0.3

0/0 interface. An initial elliptical-embedded delamination was introduced by placing two thin Teflon sheets with thickness of 20 μm at the center interface of the laminates. The dimensions of the initial delamination and laminate thickness are listed in Table 2. Ultrasonic C-scan image of the initial delaminations are shown in Figure 1, where an angle θ is defined to indicate the position of the delamination front.

The specimen was loosely set in a fixture shown in Figure 2 in order to allow in-plane movements in the fixture during the test. The diameter of the hole of the fixture was 100 mm. The specimens were pushed by a spherical steel head indenter with a diameter of 40 mm at the center of the specimen, that is, at the center of the embedded delaminated area by a cross-head speed of 0.1 mm/min. The test was suspended several times to carry out the non-destructive inspection using ultrasonic C scan to obtain the damage configuration. The specimen was reset in the fixture after the inspection so that the location of the indented point did not change.

Figure 3 shows a relation between the applied load and cross-head displacement. The loading was suspended and repeated eight times. At each trial, the final load was increased by some amount to make the delamination grow. Hardening non-linearity was found due to Herzian contact at early stage of loading and due to finite deflection of the plate at high load region. Slight stiffness reduction caused by the damage growth was observed at the large load area, but no sudden drop of the load occurred during the testing, that is, no unstable damage growth occurred. The stiffness must reduce some amount at each trial since the delaminated area increased at each trial. At each step, C-scan images were taken from both sides. The shapes of the damage was carefully measured so as to get accurate energy release rate (ERR), since the ERR was calculated based on the measured shape of the delamination using a finite element analysis as explained in the next section.

3. Finite element analysis

Finite element analysis was conducted using commercial software (Abaqus 6.7). Material properties are listed in Table 1. Eight-node isoparametric brick element was used. Geometrical non-linearity was considered, because the displacement of the specimens was not small compared to the plate thickness. A finite element model and boundary conditions are illustrated in Figure 4. The vertical displacement of the upper surface of the elements outside the fixture edge was constrained to express the loose fix of the stiff fixture. An equivalent uniform distributed load was applied at the center small portion of the top surface of the plate as shown in Figure 4 instead of considering the contact problem of spherical head. The plates were discretized according to the carefully measured shapes of the C-scan images of the delamination. The crack tip area was discretized using more than four same-width small elements in the normal direction to the crack tip line, since it was essential to get similar displacement field at the crack tip

Table 2. Dimensions of initial elliptic delaminations and plate thickness (unit: mm).

Specimen	Major diameter	Minor diameter	Thickness
E1	60	30	3.95
E2	60	30	3.98
E3	45	28	3.95

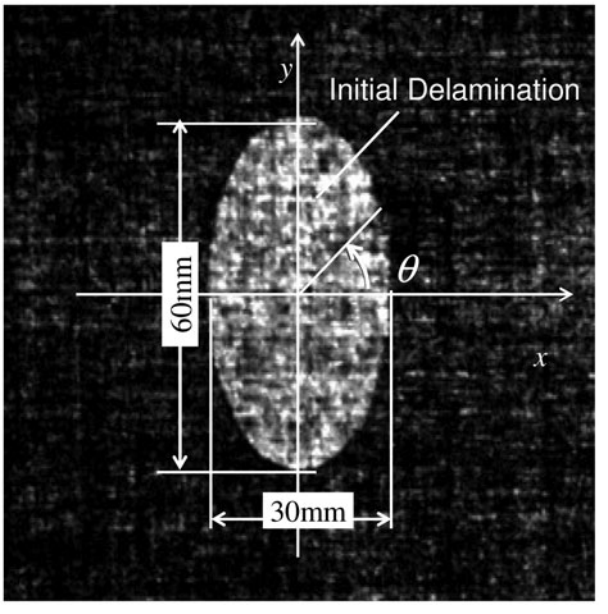

Figure 1. Ultrasonic C-scan image of initial delamination in a cross-ply specimen.

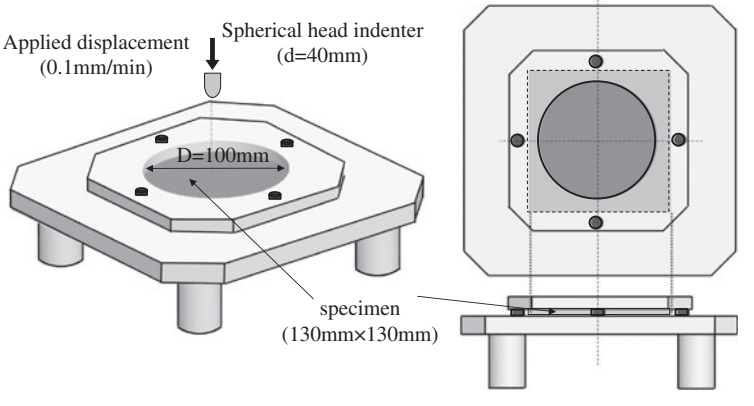

Figure 2. Test fixture and specimen.

before and after the crack growth of one element. The delamination was modeled by duplicated nodes. Each pair of the duplicated nodes except those next to the crack tip was connected by a tensionless spring to constrain only the negative relative displacement in thickness direction, that is, to prevent both the delaminated surfaces from overlapping. The spring elements had high stiffness in compressive direction and no resistance in tensile direction. Three-mode components of the ERR G_I, G_x, and G_y were calculated according to Virtual Crack Closure Technique (VCCT).[22] The finite element analysis was conducted twice. Firstly, the three components of the closing nodal force f_x, f_y, and f_z of each duplicated nodes at the delamination edge were obtained by

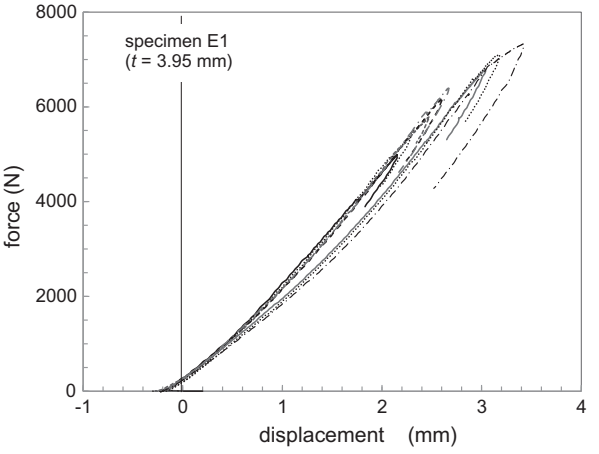

Figure 3. Relationship between load and center displacement. The loading and unloading was repeated several times with increasing the maximum load.

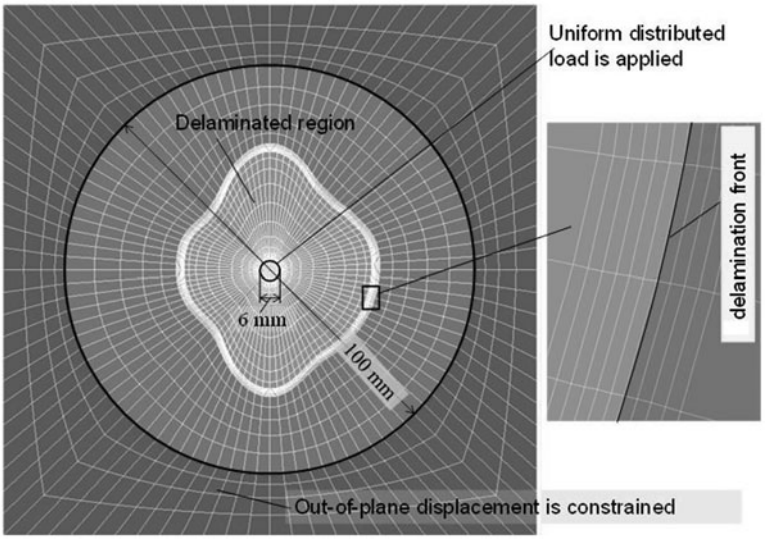

Figure 4. A finite element discretization of a damaged specimen and the boundary conditions of the laminate.

placing very stiff spring elements in x, y, and z directions between each corresponding pair of the duplicated nodes as shown in Figure 5(a). Then, the three components of the relative displacement δ_x, δ_y, and δ_z were obtained by replacing the stiff spring elements with very compliant spring elements between the same corresponding pair as shown in Figure 5(b). Using spring elements, the spring forces and the spring displacements are outputs independently from the other huge data and the following calculation of ERR can be conducted, relatively, easily. From the z, x, and y components of the nodal forces and the corresponding relative displacements, each ERR component was calculated according to the following equations.

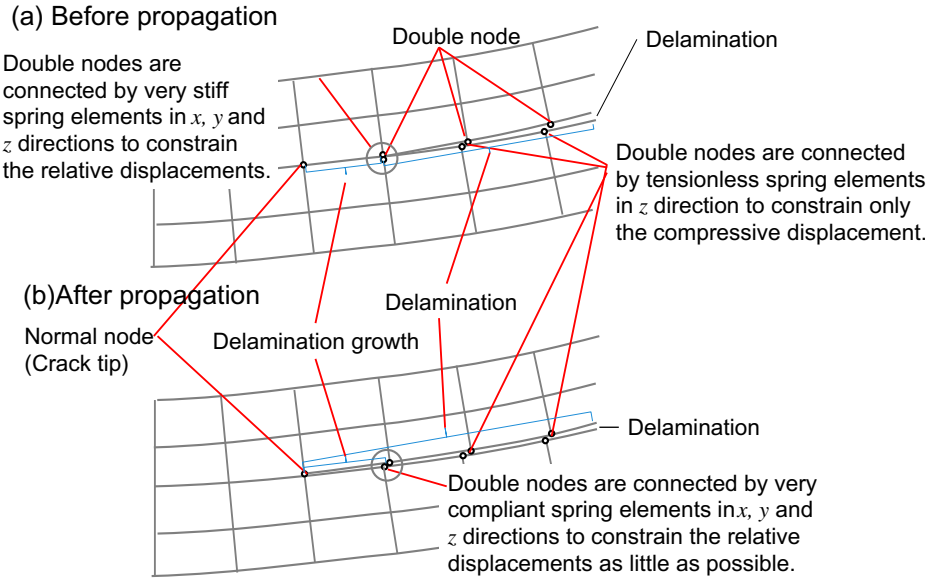

Figure 5. Finite element modeling of the delaminated portion and illustration of the VCCT.

$$G_I = \frac{1}{2A_e} f_z \delta_z, \quad G_x = \frac{1}{2A_e} f_x \delta_x. \quad G_y = \frac{1}{2A_e} f_y \delta_y \tag{1}$$

where A_e is half of the summed area of the two elements including the nodes which are released in the second analysis. If necessary, G_{II} and G_{III} components could be also calculated by multiplying the force components and the relative-displacement components after the coordinate transformation by the angle between x axis and the normal of the crack tip curve. The total ERR G_T equals the sum of the three components, that is,

$$G_T = G_I + G_x + G_y = G_I + G_{II} + G_{III}. \tag{2}$$

The load–displacement relationship of the present finite element analysis agreed well with the experiment as shown in Figure 6 when the effect of Herzian contact (initial nonlinearity) was eliminated from the experimental result.

4. Results and discussions

4.1. Damage propagation

Ultrasonic images of specimens E1 and E3 at several load levels are shown in Figures 7 and 8. The gray-colored portions are the delaminated areas. The delaminations grew with the load increase. The measured shapes of delamination fronts of the specimens E1 and E2 are indicated in Figure 9. The damage growth history is illustrated in Figure 10. The delamination edge initially spread from the center portions of the ellipse and propagated only in the horizontal direction at the interface (0/0) as shown in Figure 10(a). The propagated shapes might not be symmetric owing to the probabilistic nature of the interlaminar fracture resistance. As the delamination simply propagated, a critical ERR can be specified at this stage.

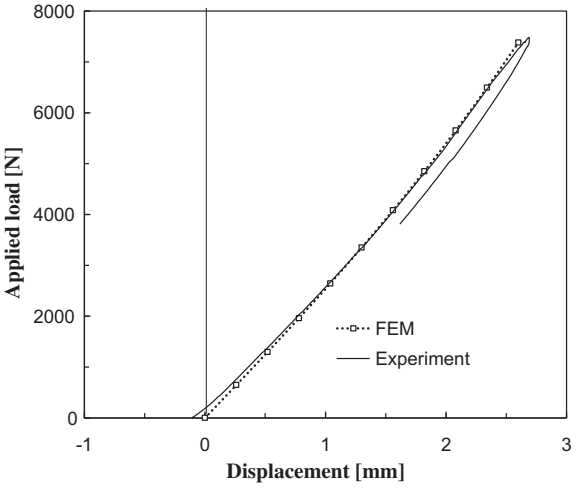

Figure 6. Comparison between the test and the numerical results.

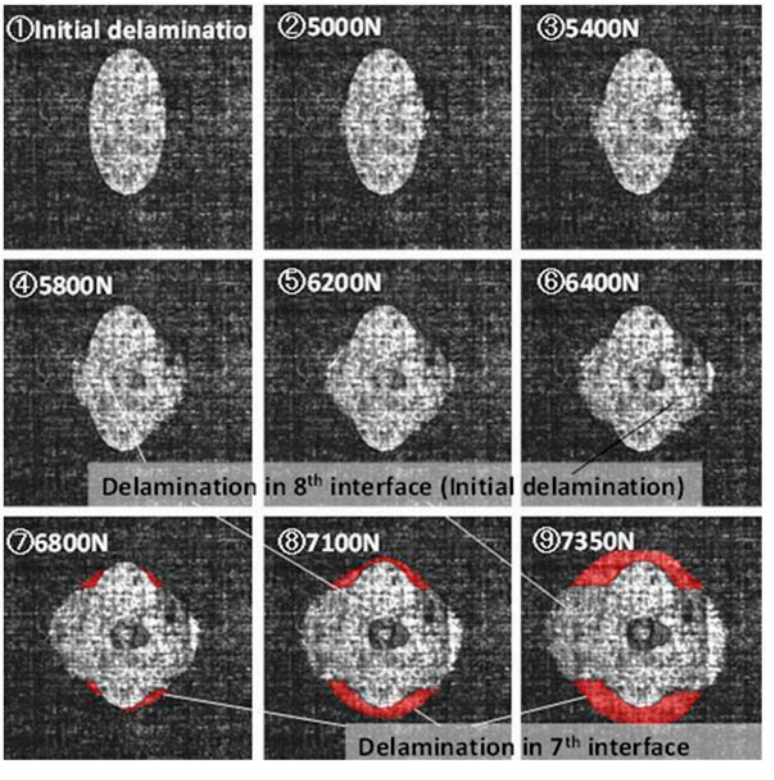

Figure 7. A delamination growth history of an initially elliptical delamination (specimen E1).

The growth along the periphery of ellipse stopped at point A as shown in Figure 10(b) for a while where the angle α_0 between the radial direction and horizontal fiber direction was sufficiently large ($\alpha_0 \sim 60°$). The stress state due to the transverse shear at this point is

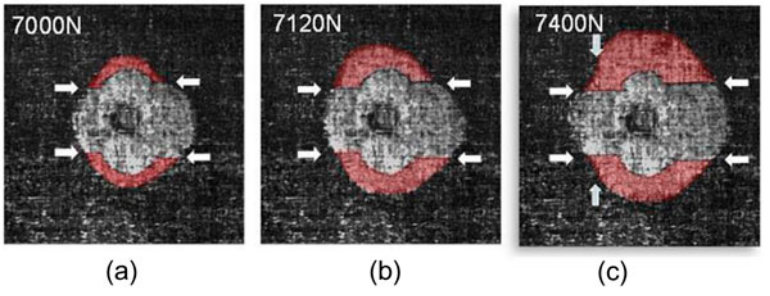

Figure 8. Damage shapes of specimens E3 at loads 7000 N, 7120 N, and 7400 N. The arrows indicate the matrix cracks.

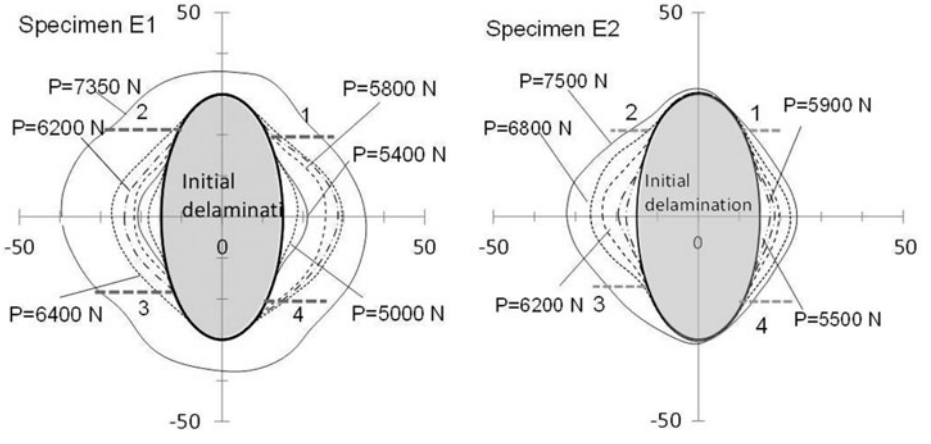

Figure 9. Measured damage growth profiles of specimens E1 and E2. The horizontal gray broken lines 1–4 indicate the position where the matrix cracks started.

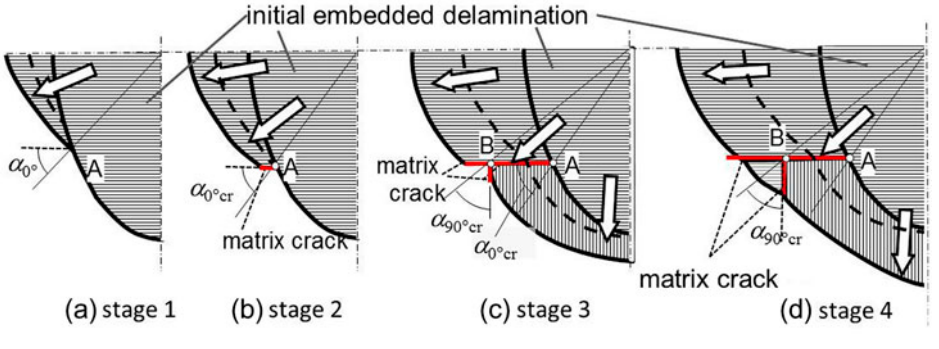

Figure 10. Illustration of three-dimensional damage growth history. Delamination migration and matrix crack growth occurred during the load increase.

shown in Figure 11. Though both the shear components τ_{zx} and τ_{zy} cause tensile stress at 45° inclined planes ahead of the crack in the layer below the delamination, only τ_{zy} can make the crack migrate into the layer. So, significance of migration can be expressed by the ERR component G_y. The migrated crack will stop at the 0/90° interface as shown in Figure 12 and it needs higher ERR to restart the propagation at the new interface inclined from the migrated matrix crack than the interlaminar fracture resistance. This may be a reason that the migrated cracks were arrested for a while.

The damage started growing in the lower interface (0/90) at the four shoulder portions of the embedded delamination (indicated by horizontal arrows). Transverse matrix cracks connected the delamination in the 0/0 interface and newly grown delaminations in the 0/90 interface at the portions as shown in Figure 13. The delaminations in the 0/90 interface seemed to grow along the edge portions of the embedded elliptical delamination and grew vertically in the fiber direction of the lamina just below.

The delamination growth was arrested again near the horizontal matrix cracks as illustrated in Figure 10(c). Vertically growing matrix cracks were observed at the area as shown in Figure 14, where angles $\alpha_{90°}$ were large (50°–60°). The mechanism is same as explained earlier in Figure 11. The damage system consisting of delaminations not only in the interface of embedded delamination but also in the interfaces below the original interface accompanying the horizontally and vertically outward-growing matrix cracks grew in the area in 45° inclined directions as shown in Figure 10(d). The projected shape of the whole damage tended to take nearly a square with rounded corners turned by 45°. The critical ERR, that is, the fracture resistance was high in the 45° inclined direction due to the three-dimensional nature of damage.

4.2. Fracture resistance of delamination growth in 0/0 interface in fiber direction

The fracture resistance obtained in the stage 1 and 2 is discussed first, when no clear matrix crack was observed and delamination propagated transversely only in the 0/0 interface. Distributions of G_T and G_y are plotted against the angle θ measured from rightward horizontal axis in Figure 15 for specimens E1, E2, and E3. As G_I was negligibly small, $G_x \approx G_T - G_y$. The x- and y-directions were the fiber direction of the 0° and 90° layers, respectively. Specimen E3 had a smaller embedded delamination. The plots of $P = 4500$ N for E1 and E2, and $P = 4000$ N for E3 are the ERR distributions before damage growth. The ERR values at these instants were lower than the interfacial fracture resistance of the specimens. The ERR values of the propagating delamination front must be the fracture resistance of the interface. The ERR values at the propagating delamination were relatively stable and ranged from 0.9 to 1.1 kJ/m^2 for specimen E1,

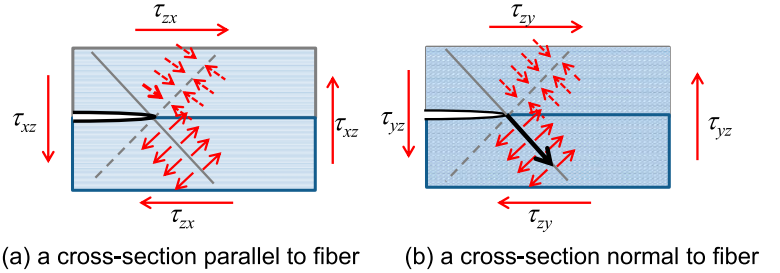

Figure 11. Fiber orientation and stress state under shear fracture condition.

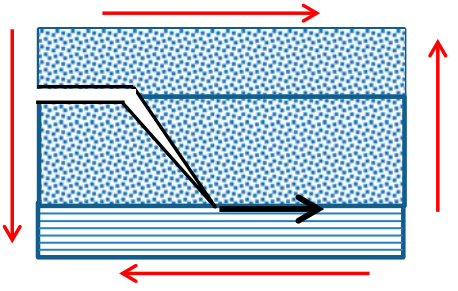

Figure 12. Deflection of migrated crack.

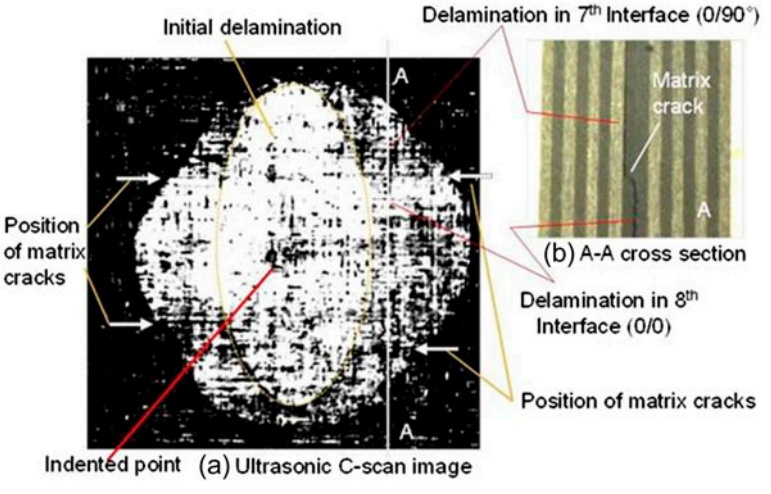

Figure 13. An ultrasonic C-scan image of E2 specimen and the photograph of a cross-section.

from the 1.05 to 1.35 kJ/m^2 for specimen E2, and from the 0.95 to 1.2 kJ/m^2 for specimen E3. Then, we determined the fracture resistance of each specimen roughly 1.0, 1.2, and 1.1 kJ/m^2, respectively. The present values are consistent with the results of ENF test ($G_{IIc\ 0/0\ \text{interface}} \sim 1.0$ kJ/m^2). The ERR obtained here can be the shear mode toughness of 0/0 interface. The total ERR remained stable at all propagating delamination front where the ERR component G_y was not high. The component increased with the load where the radial direction inclined well from the horizontal axis.

4.3. *Fracture resistance of delamination when matrix cracks occurred*

The total ERR G_T and two ERR components G_x and G_y of the specimen E1 at $P = 6400$ N are plotted against the angle θ in Figure 16. Matrix cracks originated at four positions of initial elliptic delamination as explained in Section 4.1. The four originating locations of the matrix cracks are indicated by triangular symbols and gray vertical lines. The ERR, that is, the fracture resistance became very high at these portions. It was thought to be caused by migrations of the delamination into lamina. So, it may be called the anchoring effect of the migrated crack. The ERR value of the propagating delamination between the

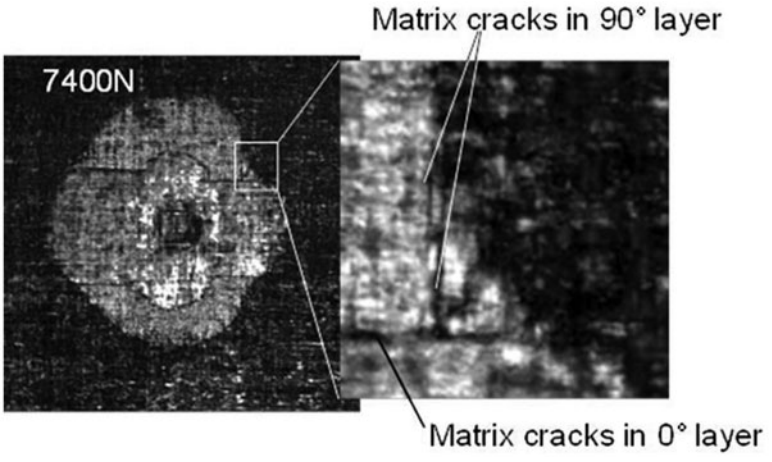

Figure 14. Vertically propagating matrix crack (Ultrasonic C-scan image of the E3 specimen taken from the back side, same specimen of Figure 8(c)).

matrix cracks was unchanged and showed a similar value as the former stage. Since the ERR was still low at the top and bottom portions of the initial delamination ($-120° < \theta < -60°$ and $60° < \theta < 120°$), the delamination could not grow yet.

The total ERR G_T and two ERR components G_x and G_y of specimen E1 at $P = 7350$ N and specimen E3 at $P = 7000$ N are plotted in Figures 17 and 18 when the whole edge of damage was growing in radial direction. The peak ERR values of specimen E3 were larger than those of E1, but both results showed similar distributions and values except the peak values. The delaminations grew at the portions indicated by striped shadow in the 0/0 interface as well as the portions indicated by crossed shadow in the 0/90° interface one layer below. Vertical gray lines indicate the locations of the matrix crack tips at this moment. The fracture resistance was very high at the delamination edges of the 0/90° interface besides the matrix cracks. Fracture resistance of simple delamination propagation is discussed first. The value G_T was comparatively consistent comparing to the data variation of ENF tests. G_x was dominant at the delaminations in 0/0 interface, while G_y was dominant at those in 0/90° interface. The fracture resistances of delamination growth in 0/0 interface and in the 0/90° were about 0.85 and 1.0 kJ/m^2 for specimens E1 and E2. (Very small value obtained at the 90° direction in Figure 18 might be caused by the measured error of the delamination profile, which had very high EER value beside this point.) ERR of 0/90° interface seemed to be a little higher than that of 0/0 interface. But the difference is considerably small compared to the variation of fracture resistance. This fact is consistent with the ENF test result shown in Table 1. SEM micrographs of the failed surfaces of 0/0° and 0/90° interfaces are shown in Figure 19. The failed surface of 0/0 interface was smooth where the propagation was parallel to the fiber (A) and some inclined damage pattern was observed where the radial direction was inclined from the fiber (B). Most of the failed surface of 0/90° interface had the pattern of 90° layer (C) and (D). It showed that the delamination propagated in the fiber direction of the 90° layer near the 90° layer. There was also an inclined damage pattern in the 0/90° interface when radial direction inclined from the vertical fiber direction.

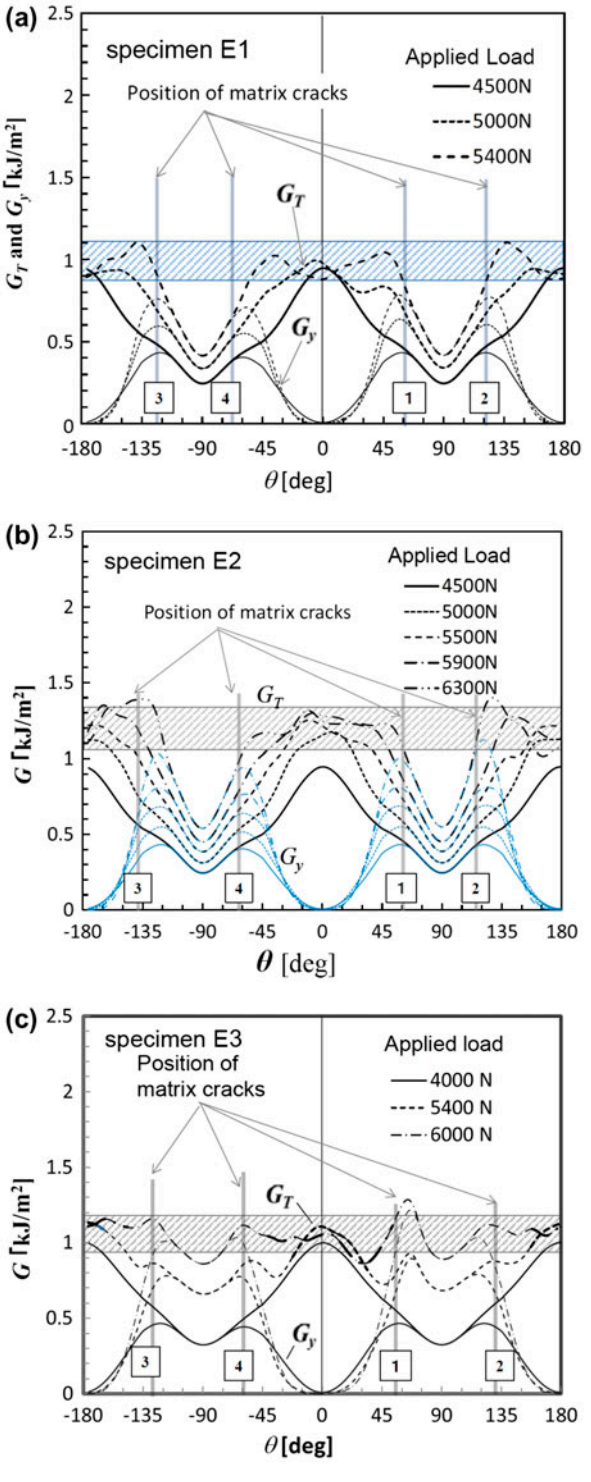

Figure 15. Total ERR G_T and its vertical component G_y for specimens E1, E2, and E3. The vertical lines numbered 1–4 indicate the positions from which the transverse matrix cracks originated.

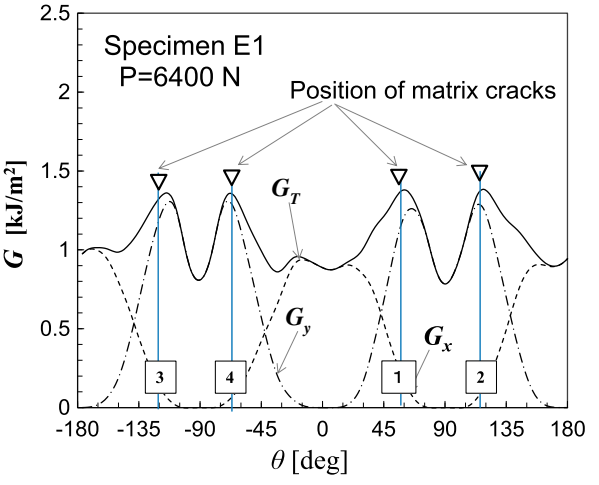

Figure 16. Total ERR G_T and its x and y components G_x and G_y of specimen E1 when $P = 6400$ N. The gray vertical lines with a number indicate the positions of the matrix cracks in 0° layers.

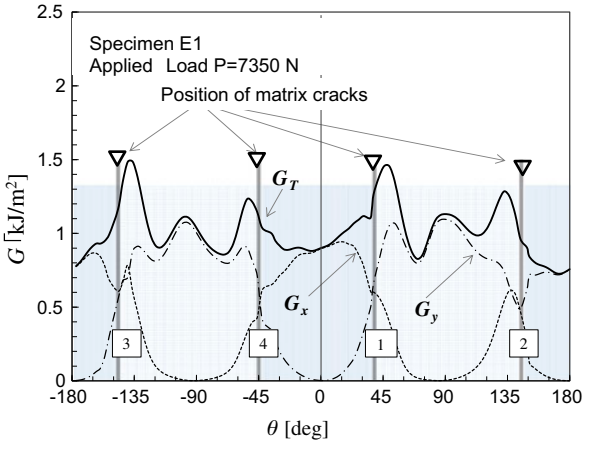

Figure 17. Total ERR G_T and its two components G_x and G_y of specimen E1 at $P = 7350$ N (whole delamination edges were propagating). The delamination propagates in 0/0 interface in stripe shade areas and the delamination grows in 0/90° interface in check shade areas. The marks-indicate the positions of the matrix crack tips in the 0° layer.

The total ERR G_T and two ERR components G_x and G_y of specimen E3 at $P =$ 7400 N are plotted in Figure 20. The ERR at the edge of horizontal matrix crack reduced with the damage growth. The ERR increased at the edge of the newly grown vertical matrix cracks. At this points, the delamination in the 0/90° interface started to migrate into the 0° layer below.

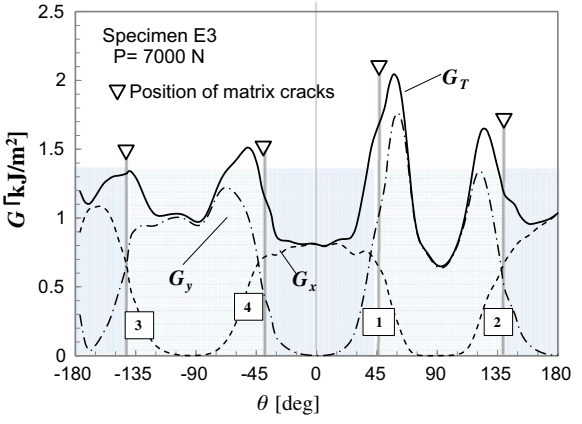

Figure 18. Total ERR G_T and its two components G_x and G_y of specimen E3 at $P = 7000$ N (whole delamination edges were propagating). The delamination propagates in 0/0 interface in stripe shade areas and the delamination grows in 0/90° interface in check shade areas. The marks indicate the positions of the matrix crack tips in the 0° layer.

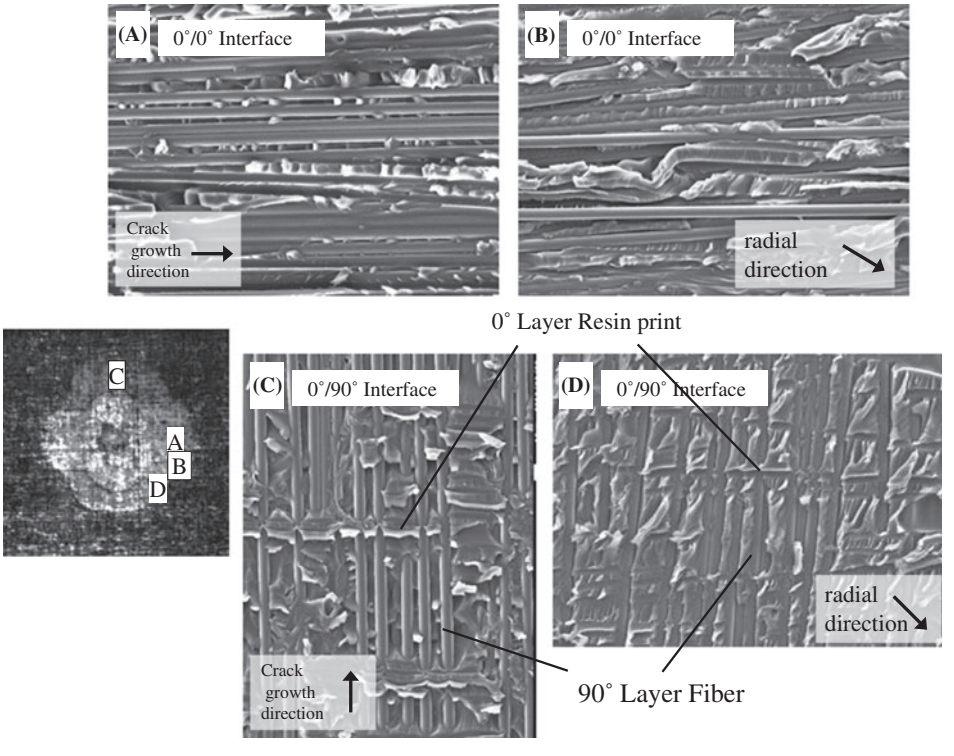

Figure 19. SEM micrographs of the fracture surfaces of specimen E3.

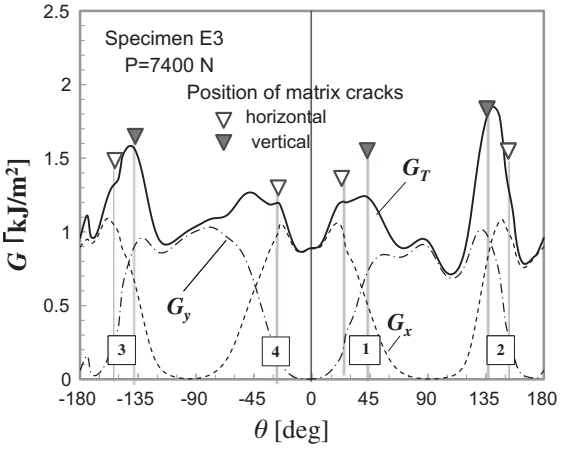

Figure 20. Total ERR G_T and the two components G_x and G_y of specimen E3 when whole delamination edges were propagating. The marks ▽ and ▼ indicate the positions of the propagated matrix cracks in 0° and 90° layers, respectively.

4.4. *Fracture resistance components and three-dimensional damage growth*

The component G_y was large in the directions of the matrix crack-originating point for all specimens at stage 1 as shown in Figure 15. So, the matrix crack origination is strongly governed by the ERR component G_y normal to the fiber direction. Once the delamination started migrating into the ply, delamination growth was arrested and G_T became very large. The condition of matrix crack initiation, that is, the migration is roughly $G_{ycr} \sim 1.0\,\text{kJ/m}^2$ from Figures 16 and 17. The initiation condition of new delamination growth in vertical direction in 0/90° interface from the edge of the matrix cracks is $G_{Tcr} > 1.5\,\text{kJ/m}^2$ from the figures. The farther growth of delamination in 0/90° interface may be controlled by G_T. The component G_x normal to the fiber direction must be small so that another migration would not occur in the 90° layer.

Farther growth of damage made the angle of the horizontal matrix crack and radial direction reduce. At 0/90° interface beside the matrix crack, the component G_x increased and G_y reduced with the growth of the delamination. This ERR component G_x, the shear component normal to the fiber of the 90° layer below, reached about $1\,\text{kJ/m}^2$. This caused another migration into the 90° layer. The delamination was again arrested at this area.

5. Conclusion

Stable interfacial failure under mixed shear fracture mode was experimentally observed using indentation test and the fracture resistance under general shear-mode stable crack propagation condition was estimated using a finite element method. The fluctuation of the total fracture resistance was not significant along the crack tip under the present shear mode test except the delamination migration area. As long as the shear mode component normal to the fiber was relatively small compared to the component parallel to the fiber, the total fracture resistance G_T was not directly dependent on the ratio of mode components. The delamination migration into the lamina tended to start at the place where the component of the fracture resistance normal to the fiber was large. At the migration points, the fracture resistance G_T locally increased owing to the anchoring effect at the migrating point.

Acknowledgment

We would like to acknowledge the support of Japan Society Promotion of Science, Grants in Aid for Scientific Research (C) 24560111, and Japan Aerospace Exploration Agency (JAXA) as co-research project.

References

[1] Whitney JM. Stress analysis of the double cantilever beam specimen. Compos. Sci. Technol. 1985;23:201–219.
[2] Robinson P, Song DQ. A modified DCB specimen for mode I testing of multidirectional laminates. J. Compos. Mater. 1992;26:1554–1577.
[3] de Morais AB, de Moura MF, Marques AT, deCastro PT. Mode-I interlaminar fracture of carbon/epoxy cross-ply composites. Compos. Sci. Technol. 2002;62:679–686.
[4] Carlsson LA, Gillespie JW, Pipes RB. On the analysis and design of end notched flexure (ENF) specimen for measuring mode II fracture toughness. Compos. Sci. Technol. 1986;20:594–604.
[5] Carlsson LA, Gillespie JW, Trethewey BR. Mode II interlaminar fracture of graphite/epoxy and graphite/PEEK. J. Reinf. Plast. Compos. 1986;5:170–187.
[6] Ozdil F, Carlsson LA, Davies P. Beam analysis of angle-ply laminate end-notched flexure specimens. Compos. Sci. Technol. 1998;58:1929–1938.
[7] Reeder JR, Cews JH. Mixed-mode bending method for delamination testing. AIAA J. 1990;28:1270–1276.
[8] Benzeggagh ML, Kenane M. Measurement of mixed-mode delamination fracture toughness of unidirectional glass/epoxy composites with mixed-mode bending apparatus. Compos. Sci. Technol. 1996;56:439–449.
[9] Becht G, Gillespie JW. Design and analysis of the crack rail shear specimen for mode III interlaminar fracture. Compos. Sci. Technol. 1988;31:143–157.
[10] Donaldson SL. Mode III interlaminar fracture characterization of composite materials. Compos. Sci. Technol. 1988;32:225–249.
[11] Robinson P, Song DQ. The development of an improved mode III delamination test for composites. Compos. Sci. Technol. 1994;52:217–233.
[12] Li J, Lee SM, Lee EW, O'Brien TK. Evaluation of the edge crack torsion (ECT) test for mode III interlaminar fracture toughness of laminated composites. J. Compos. Technol. Res. 1997;19:174–183.
[13] Suemasu H. On an experimental method to measure the mode-III interlaminar fracture toughness of composite laminates. Compos. Sci. Technol. 1999;59:1015–1021.
[14] Szekrényes A. Delamination fracture analysis in the G_{II}–G_{III} plane using prestressed transparent composite beams. Int. J. Solids Struct. 2007;44:3359–3378.
[15] de Morais AB, Pereira AB. Mixed mode II + III interlaminar fracture of carbon/epoxy laminates. Compos. Sci. Technol. 2008;68:2022–2027.
[16] Suemasu H, Kondo A, Gozu K, Aoki Y. Novel test method for mixed mode II and III interlaminar fracture toughness. Adv. Compos. Mater. 2010;19:349–361.
[17] Sjogren A, Asp LE. Effects of temperature on delamination growth in a carbon/epoxy composite under fatigue loading. Int. J. Fatigue. 2002;24:179–184.
[18] Trakas K, Kortschot MT. The relationship between critical strain energy release rate and fracture mode in multidirectional carbon-fiber/epoxy laminates. In: Armanios E, editor. Composite materials: fatigue and fracture. Vol. 6. ASTM STP 1285. West Conshohocken (PA): ASTM; 1997. p. 283–304.
[19] Kim BW, Mayer AH. Influence of fiber direction and mixed-mode ratio on delamination fracture toughness of carbon/epoxy laminates. Compos. Sci. Technol. 2003;63:695–713.
[20] Li X, Carlsson LA, Davies P. Influence of fiber volume fraction on mode III interlaminar fracture toughness of glass/epoxy composites. Compos. Sci. Technol. 2004;64:1279–1286.
[21] Greenhalgh ES, Rogers C, Robinson P. Fractographic observations on delamination growth and the subsequent migration through the laminate. Compos. Sci. Technol. 2009;69: 2345–2351.
[22] Shivakumar KN, Tan PW, Newman JC. A virtual crack-closure technique for calculating stress intensity factors for cracked three dimensional bodies. Int. J. Fract. 1988;36:R43–R50.